Scattering and absorption in 2D optics

Mariani, F.

Angle resolved transmission through sparse metal hole arrays

We present the first angle resolved measurements of extraordinary optical transmission (EOT) through hole array gratings in a gold film. Varying the lattice spacing of the arrays and looking at higher diffraction orders, we retrieve the angular emission pattern of the constituent holes with better signal to noise ratio than with single-hole experiments. We present a method to determine separately the angular dependence of the direct and resonant contribution to EOT by using the spectral features of the diffraction orders together with an established model. The comparison of our results with the known angular transmission of a single hole in a metal film yields a good agreement for s-polarized light. Deviations are found for illumination with p-polarized light and we address the discrepancy with Coupled Mode Model calculations and Finite Difference Time Domain simulations. These measured deviations are currently not fully understood.

This chapter is published as:
F. Mariani, F. de León-Pérez, K. J. A. Vendel, L. Martín-Moreno, and M. P. van Exter, Optics Express **25**, 9061 (2017)

3.1 Introduction

Metal nano-structures can strongly localize optical fields in a charge-field coupled oscillation at the metal-dielectric interface, or surface plasmon (SP). These surface waves are important in several applied fields like photonic devices [1], biosensing [2] or solar cells [3]. The shape of nano-structure defines the character of the SPs, which can be either a resonance localized on nanoparticles [4] or distributed on periodic structures [5].

Nano-holes arrays are a well known class of periodic structures since the discovery of Extraordinary Optical Transmission (EOT) on metal hole gratings [6], an intriguing effect emerging from the collective action of many holes in a lattice structure. Extensive studies were conducted to understand how this phenomeon depends on the material [7], size [8, 9] and shape [10] of the holes and how surface waves propagate and couple to contribute to the spectral features of EOT [11, 12]. The physical picture of EOT is based on transmission of the electromagnetic field through nanoholes aided by resonant surface waves of the patterned structure[13]. These waves can be understood, in metal films, from the multiple scattering of SPs on holes at the flat interfaces; plasmons play the biggest role [14], together with the so called quasi-cylindrical wave (QCW) [15, 16, 17, 18].

Transmission studies on metal hole arrays are generally performed in collinear transmission geometry as the typically used structures have square symmetry with lattice constant which only allows one diffraction order at the wavelength of study. We use here metal hole arrays with a rectangular unit cell, one lattice constant being an integer multiple of a fixed spacing used in the orthogonal direction (see inset of Fig. 3.1(a)). An increasing number of diffraction orders appears for increasing lattice constant and this makes it possible to give a first description of the angular emission properties of EOT in the full scattering plane, by angularly resolving the diffraction orders in transmission.

The information we obtain allows to reconstruct the angular emission profile of a single hole. The scattering properties of single holes in metal have been measured and modelled for excitations from plane waves [19, 20], looking at the angularly resolved transmission. We now show how from transmission measurements of rectangular arrays of holes it is possible to separate the contribution of excitation from plane waves and SPs, employing an established model for EOT. The resulting signal-to-noise ratio in our experiment is better

than in experiments on single holes since more holes contribute to transmission and the intensity is concentrated in well defined directions by interference. In our study we find a polarization dependent deviation of the angular emission profile as compared to existing theory for diffraction from single holes in metal. We report it here and speculate on the possible cause of this unexpected behaviour.

3.2 Hole arrays and setup

Our hole arrays are obtained on a 170 nm thick gold layer, evaporated on a substrate of BK7 glass ($n_d = 1.51$) and are capped by a 20 nm chromium layer to quench SPs at the gold-air interface. The holes, produced with standard e-beam lithography and lift-off techniques, have a diameter of 165 nm and are arranged in chains with a fixed lattice constant $a_0 = 450$ nm. A two-dimensional rectangular hole array is constructed from multiple chains repeated parallel to each other at a spacing of qa_0, with the spacing factor $q = 1 - 14$ identifying each array (see inset in Fig. 3.1(a) for q=2). All the final arrays have the size of a square with side of 400 μm.

The experimental setup is shown in Fig. 3.1(a). We illuminate the sample at normal incidence with a white light source (Energetique LDLS EQ-99) coupled via a multimode fiber (diameter 200 μm) imaged on the sample in a spot of 300 μm diameter. The angle resolved transmission $T(\lambda, \theta)$ of the hole arrays is collected using a computer controlled goniometric stage rotating in the xz plane. The detection optics is mounted on this stage and consists of two lenses in 4f-configuration, imaging a second multimode fiber (diameter 400 μm) on the sample in a spot as large as 1.2 mm; this magnification is chosen to make the setup less sensitive to misalignments during angular scans. The collected light is spectrally analyzed with a fiber-coupled spectrometer (Ocean-Optics USB2000). Polarization resolved measurements are made possible by two polarizers placed in both excitation and detection arms. Hole arrays are always oriented with hole chains along the $\hat{y}$ axis, as shown in the inset of Fig. 3.1(a). We define the scattering angle θ as the angle with the surface normal (see Fig. 3.1(a)) and the p(s)-polarization of the light for the E field oriented along $\hat{x}(\hat{y})$.

The excitation light has a numerical aperture $\mathrm{NA}_{in} = 0.01$; this is small enough to ensure the spatial coherence required in our experiment, but large enough for the total intensity not to be reduced by diffraction. The excitation

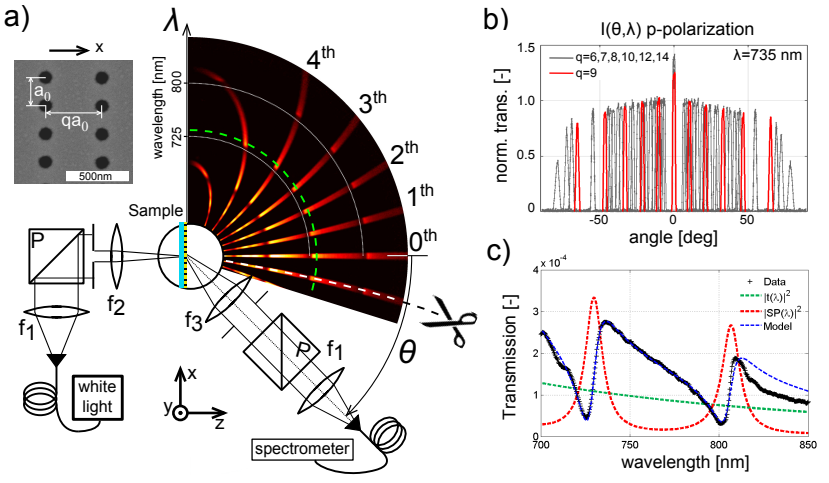

Figure 3.1: (a) The goniometric setup used in the experiments. The sample is illuminated at normal incidence ($\mathrm{NA}_{in} = 0.01$) with a fiber-coupled white-light source. A second telescope ($\mathrm{NA}_{out} = 0.03$) scans, on a rotating stage, a semi-circle in the xz plane and collects the transmitted light at scattering angle θ. Focal lengths are $f_1 = 50$ mm, $f_2 = 75$ mm, $f_3 = 150$ mm. Polarizers allow polarization-resolved study of the transmission. The false color plot reports the transmitted intensity $I(\theta, \lambda)$ for the $q = 9$ array. The inset shows a detail of SEM image of sample with $q = 2$. (b) Cross-cuts of $I(\theta, \lambda)$ at fixed $\lambda = 735$ nm, i.e. along the green dashed arc indicated in a), for all the measured q spacings. (c) Transmission spectrum for the 1^{st} diffraction order of the $9a_0$ array extracted along the white dashed line in a). The data are fitted with the model in Eq. (3.1). From the calculated parameters it is possible to separate the direct transmission $|t|^2$ (green dotted lines) and the resonant contribution $|SP|^2 = \left|s/(u^{-1} - \sigma)\right|^2$ (red dotted lines).

NA also defines the angular width of the diffraction orders. The collection optics has $\mathrm{NA}_{out} = 0.03$, defining an acceptance angle wider than the angular width of the excitation.

3.3 Theoretical model of spectral and angular transmission

With the purpose of experimentally studying the angular dependence of EOT, we use analytical models to interpret both the spectral and angular degrees of freedom of our transmission measurements. We compare our results with existing theories, confirmed by experiments, for the EOT spectra and for the optical diffraction from small holes on metal films.

For the spectral response we use the model presented in [14] which explains the Fano shape of the resonances in the EOT transmission spectrum $T(\lambda)$. This model applies to the case of normal illumination and for polariza-

tion parallel to one of the lattice axes. In the model the array is considered as a one-dimensional grating of chains of holes. The incident light has two effects: a fraction of it is directly transmitted through the holes (non-resonant contribution) and part of it excites SPs propagating over the metal-dielectric interface in the direction of the incident light polarization. The latter scatter at the hole chains, being partially transmitted and reflected, and a SPs resonant field builds up, similarly as in a distributed Fabry-Perot cavity. The SPs field partially leaks through the holes and contributes to the transmission. We indicate with $t(\lambda)$ the transmission amplitude of the non-resonant field, and with $s(\lambda)/(u^{-1}(q) - \sigma)$ the transmission amplitude originating from the resonant SPs field. The expression at the denominator accounts for the multiple roundtrips of SPs over the array and includes a SP-SP scattering coefficient $\sigma \leq 1$ and the phase delay and amplitude loss $u(q) = \exp(ik_{spp}qa_0)$ due to the SPs propagation over the distance between two chains; in particular the function $u(q)$ defines the position of the resonances. The two transmission amplitudes interfere and add up coherently, yielding the intensity transmission spectrum [18]:

$$T(q, \lambda) = q^{-2} \left| t(\lambda) + \frac{s(\lambda)}{u^{-1}(q) - \sigma} \right|^2 \tag{3.1}$$

The pre-factor q^{-2} gives the scaling of the transmission intensity on the holes surface density. We take $t(\lambda)$ real valued and dependent on wavelength as $t(\lambda) \propto \lambda^{-2}$ and $s(\lambda)$ complex valued and proportional to λ^{-4}. This choice for the dependence on wavelength is supported by previous works [19, 5, 14]. We refer the reader to [14] for additional details.

The model in Eq. (3.1) has been used in an experimental study on EOT at 0^{th} diffraction order [18] (our coefficient $s(\lambda)$ is equivalent to the product $2\alpha\beta$ in the original publication). We will extend it to higher diffraction orders by introducing an angular dependence for the coefficients $t(\lambda)$ and $s(\lambda)$; these separately describe the angular emission properties of a single hole chain under the excitation of, respectively, an incident light wave or by a SP wave. As these are two physically distinct excitations, they can in principle manifest different angular emission profiles.

The angular response of an array of coherent emitters can be written as the product of two factors: (i) the structure factor $S(\theta)$ of the hole array (interference) and (ii) the form factor of the individual emitters (diffraction) which in our case are single nano-holes. The structure factor is peaked at the reciprocal lattice sites, as an excitation of wavevector $\vec{k}_{in}$ will only scatter in

directions given by $\vec{k}_{out} = \vec{k}_{in} + \vec{G}$, with $\vec{G}$ a vector of the reciprocal lattice [5]. For the transmission form factor of an individual hole in metal we use an analytical theory developed in the framework of the Coupled Mode Method (CMM) [20] and based on expansion of the field in relevant optical modes. The solutions we use here apply to subwavelength holes, where the transmission is dominated by the fundamental mode TE_{11}. It yields the transmitted intensity from a single hole as function of angle $I_\pi(\theta)$, with θ the scattering angle and $\pi = p, s$ the polarization of the incident electric field. For holes with radius $r \ll \lambda$ the contributions from p and s waves to the normalized scattering cross-section, defined as the power radiated to the far-field per unit of solid angle, normalized to its value for $\theta = 0$ read [20]:

$$\frac{I_p(\theta)}{I_p(0)} = \frac{|1+z_s|^2\cos^2(\theta)}{|\cos(\theta)+z_s|^2}\frac{4{J_1}^2(\Phi)}{\Phi^2} \simeq \frac{|1+z_s|^2\cos^2(\theta)}{|\cos(\theta)+z_s|^2}\left(1-\frac{\Phi^2}{4}\right) \tag{3.2}$$

$$\begin{aligned}\frac{I_s(\theta)}{I_s(0)} = \frac{|1+z_s|^2\cos^2(\theta)}{|1+z_s\cos(\theta)|^2}\frac{4{J_1'}^2(\Phi)}{(1-\Phi^2/u^2)^2} \simeq \\ \frac{|1+z_s|^2\cos^2(\theta)}{|1+z_s\cos(\theta)|^2}\left(1-\left(\frac{3}{4}-\frac{2}{u^2}\right)\Phi^2\right)\end{aligned} \tag{3.3}$$

where we define the ratio of the surface impedances $z_s = \sqrt{\epsilon_d}/\sqrt{\epsilon_{metal}}$, with ϵ_d and ϵ_{metal} permittivities respectively of the dielectric half space and the metal, and where $u \simeq 1.84$ is the first root of the Bessel function $J_1(u) = 0$ and $\Phi = kr\,\sin(\theta)$, with $k = 2\pi/\lambda$ and r the effective radius of the hole, also including field penetration depth in the metal.

The first terms in Eqs. (3.2)–(3.3) describe the angular emission of an infinitesimally small hole in a metal (dipole approximation). For a perfect conductor $\epsilon_{metal} \to -\infty$, the emission profile is that of a magnetic dipole with $I_p(\theta) \simeq 1$ and $I_s(\theta) \simeq \cos^2(\theta)$ [19]. The second term in the equations introduces a (Fraunhofer-like) correction accounting for the shape of the field inside the hole. The added Taylor expansions indicate the order of the correction for small values of Φ.

We have checked the applicability of Eqs. (3.2)–(3.3) by analyzing our system with the Coupled Mode Method (CMM) and by performing finite-difference time domain (FDTD) simulations. The CMM relies on a modal expansion of the EM fields, where the dielectric properties of the metal are approximately treated via the surface impedance boundary conditions [21]. Perfect electric conductor (PEC) boundary conditions have been used at the

lateral walls of the holes for the sake of analytical simplicity. Nevertheless, the real penetration of the field into the metallic walls is taken into account by enlarging the radius of the hole by 1.9δ, where $\delta = \lambda/\left[2\pi \mathrm{Im}(\sqrt{\epsilon_{metal}})\right]$ is the skin depth (an enlargement of 1.5-1.9δ improves the agreement with first principle calculations [20]). Numerical simulations using the CMM are in good agreement with both experimental results and rigorous calculations for the angular diffraction pattern of single holes [20] and the total transmission of hole arrays [22]. For sufficiently small hole diameters, the transmission process is controlled by the fundamental waveguide mode (TE_{11}) alone [22]. Here the dielectric constant of gold has been taken from the experimental data reported in [23].

To understand the energy distribution in the diffraction orders we recall that, for a hole array, the transmission angular intensity distribution is written as $I_\pi^{ARRAY}(\theta) = I_\pi(\theta)S(\theta)$. An array of N rows under uniform illumination has structure factor $S(\theta) = \sin^2(\alpha N \sin(\theta))/\left(N \sin(\alpha \sin(\theta))\right)^2$ with $\alpha = k n_d q a_0/2$. The angular positions of the diffraction maxima θ_m are obtained at the zeros of the denominator of $S(\theta)$, i.e. for $\alpha \sin(\theta_m) = m\pi$ (Bragg condition at normal incidence). A diffraction peak has a width $\Delta(\theta_m)$, which we approximate as half the distance between the two closest minima; these occur for $\alpha \sin(\theta) = (m \pm N^{-1})\pi$, giving $\Delta(\theta_m) \simeq \pi/(\alpha N \cos(\theta_m))$. The peak width increases with diffraction angle as $1/\cos(\theta_m)$ and consequently also the power emitted in each diffraction maxima $P_\pi(\theta_m) \approx I_\pi^{ARRAY}(\theta_m)\Delta(\theta_m)$ retains the factor $1/\cos(\theta_m)$ and scales accordingly.

3.4 Experimental results

We measured the transmission of the hole arrays on both the glass and the air side, with both p and s polarizations. Measurements with crossed polarizers show that no depolarization occurs in our system within experimental error. We don't show here results for the transmission on the glass side: the measured intensities in this case need to be corrected for Fresnel transmittance coefficients for passage of transmitted light through the glass-air interface, but most importantly total internal reflection (TIR) limits the accessible angular range to the critical angle $\theta_{TIR} = \arcsin(1/n_d) = 41.4°$ for transmission in the glass (for $n_d = 1.51$). This makes the experimental dataset incomplete and less useful when compared to the model in Eqs. (3.2)–(3.3).

The two main ways of studying the transmission function $T(\lambda, \theta)$ are indi-

cated by the two dashed curves in the false-color plot in Fig. 3.1(a). The first way is looking at $T(\lambda, \theta)$ at constant wavelength (dashed green semi-circle); the angular response of the system results in multiple peaks corresponding to the different diffraction orders, as shown in Fig. 3.1(b) for different values of the spacing factor q. Diffraction orders for different lattice constant spacings are located at different angular positions, thus providing an angular sampling of the transmission. From Fig. 3.1(b) one notices an excess of measured intensity for the diffraction order at $\theta = 0$: this is caused by light transmitted through the metal film, as also confirmed from FDTD calculations. In order to correctly compare different arrays, we normalize $T(\lambda, \theta)$ by $T(\lambda, 0)$ but by the average value for the $\pm 1^{st}$ orders.

The second way to study the transmission function is by cross-cutting it along the m^{th} diffraction order using the Bragg condition at normal incidence $\sin(\theta_m(\lambda)) = m\lambda/(qa_0)$, as indicated in Fig. 3.1(a) in white dashed line. This highlights the spectral response of the array, which contains characteristic Fano-type resonance peaks of EOT [14], as shown in Fig. 3.1(c).

p-polarization. When illuminating the array with p-polarized light the resulting SPs mainly propagate along $\hat{x}$, being this the direction of the electric field. A resonance is obtained for the optical frequency that satisfies the condition $q\lambda_{SP} = qa_0$, with λ_{SP} the SP wavelength at the metal-glass interface. This is the SP resonance we focus on in this work, shown in Fig. 3.1(c). It is centred at $\lambda \simeq 726$ nm and its spectral position is almost independent on the value of q. The additional resonance at longer wavelengths satisfies instead the condition $(q-1)\lambda_{SP} = qa_0$ and its position is red-shifted with increasing q.

We analyse the transmission spectra of each diffraction order using the model in Eq. (3.1), in a wavelength interval around 726 nm that includes the steep edges of the neighbouring resonances. For faster convergence we fix the value of σ, which quantifies the effect of SP scattering and only depends on the size of the hole, to an averaged value obtained when fits are run with it as a free parameter. An example of the results of the fits is included in Fig. 3.1(c) with separate plots for the direct and the resonant contributions; we note that the transmission spectra only show SPs resonances at the metal-glass interface. Resonant contributions from SPs at Cr-air interface are not visible, as expected. The parameters interesting for our study are the calculated fit parameters $t(\theta)$ and $s(\theta)$ which we normalize, for each array, by their values for the 1^{st} diffraction order. We report the result in Fig. 3.2 for all measured

diffraction orders of a set arrays of different spacing.

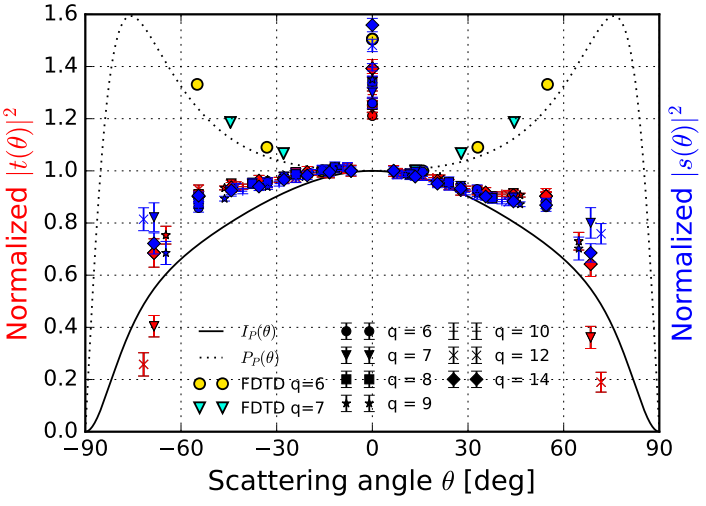

Figure 3.2: Angular dependence of the parameters $|t(\theta)|^2$ (red symbols) and $|s(\theta)|^2$ (blue symbols), derived by fitting the model in Eq. (3.1) to the transmission diffraction orders measured for p-polarization on the air side of hole-arrays. Data from different arrays are normalized to the value for first orders; note the excellent consistency of parameters from arrays of different q-values. The excess intensity at $\theta = 0$ is due to incomplete absorption of light passing through the gold film. We report for comparison $I_p(\theta)$ curve from Eq. (3.2) in solid line and, in dotted line, the curve including the correction with factor $\cos(\theta)^{-1}$ computed in Sec. 3.3 and discussed in Sec. 3.5. The latter is in excellent agreement with FDTD calculations, shown with yellow and cyan symbols, for the power in each diffraction order.

Two important observations can be done on Fig. 3.2. First, all the normalized values of the fit parameters $|t(\theta)|^2$ and $|s(\theta)|^2$ obtained from different arrays are in excellent agreement and consistently show the same angle dependence. This confirms the adopted experimental method and the relevance of the obtained angular emission profile after the analysis with the EOT model. Second, the calculated data points for $|t(\theta)|^2$ and $|s(\theta)|^2$ are superimposed on each other. We thus find that the angular emission profile is the same for excitation by either resonant SPs or by direct non-resonant optical transmission through the holes. The two parameters are not superimposed at the largest scattering angles because the angle dispersion deforms the transmission curve for the longest wavelengths of the fitting interval, reducing agreement with the model.

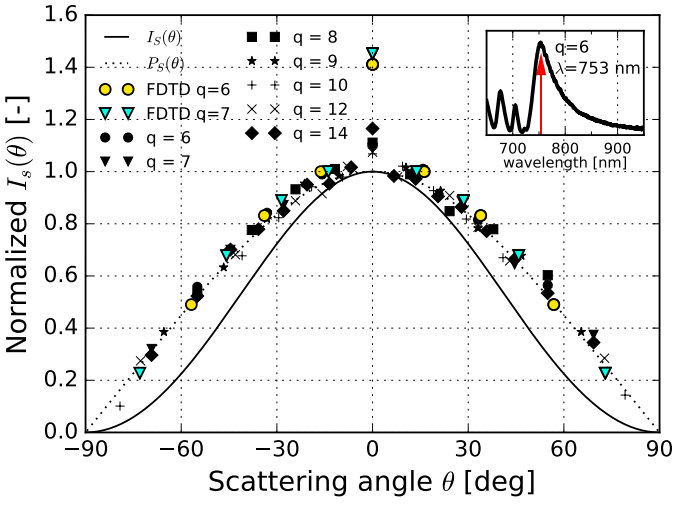

Figure 3.3: Peak values for the resonance in the transmission spectra at different diffraction orders obtained with illumination with s-polarized light (peak position around 750 nm, shown in the inset) for detection on the air side. The solid curve shows the single-hole diffraction obtained with Eq. (3.3), while the dotted curve shows this result after correction by a factor $\cos(\theta)^{-1}$ computed in Sec. 3.3 and discussed in Sec. 3.5.
The latter curve overlaps with both the experimental data, as expected, and with the results of FDTD calculations of the power in each diffraction order, shown with yellow and cyan symbols.

s-polarization. In Fig. 3.3 we report the normalized transmission data for s-polarization. Illumination with s-polarized light generates SPs waves propagating mainly along the $\hat{y}$ direction, i.e. along the chains. These SPs scatter frequently on holes belonging to the same chain and generate a distinct resonance, visible in the inset in Fig. 3.3. Holes belonging to the same chain are close enough for quasi-cylindrical waves to play a role in the hole-hole interaction [18], with possible effects on the transmission spectrum. The inset also shows additional resonances at shorter wavelengths very close to the main resonance, originating from SPs propagating at a small angle with respect to $\hat{y}$. These additional resonances make an analytical model more complicated in the case of s-polarization; we thus study the angular dependence of s-polarized light by taking the peak value of the transmission intensity. This is justified as the main resonance peak dominates the transmission spectrum.

3.5 Discussion

We explain the almost perfect match of the angular behaviour of the fit parameters $|t(\theta)|^2$ and $|s(\theta)|^2$ as follows: for detection on the air side both excitation sources, incident plane wave (direct transmission) and SP field on the glass side, first need to couple to the fundamental TE_{11} mode of the hole before being transmitted at the air side. As a result, the final angular behaviour is only dictated by the way the fundamental hole mode couples to the radiating modes on the detector side. This restriction applies also to the contribution of the quasi-cylindrical wave propagating on the glass side which is expected, at a specific wavelength, to show the same transmission angular dependence.

For a correct comparison of experiment and theory, we note that our setup measures an angular intensity integrated over the detection angle, i.e. an optical power $P(\theta)$. The width of each diffraction orders is determined by the excitation NA and increases with diffraction angle by a factor $1/\cos(\theta)$, as calculated in Sec. 3.3. For our geometry ($NA_{in} = 0.01$, $NA_{out} = 0.03$) diffraction maxima at $\theta < \arccos(NA_{out}/NA_{in}) \simeq 70^\circ$ are completely collected by the detection aperture; for higher scattering angles the detection optics partially crops the transmitted light and the measured optical power is slightly underestimated.

Measurements for s and p polarization show very different agreements to intensity and power curves calculated with single hole diffraction theory. For s-polarization, the experimental data shown in Fig. 3.3 perfectly overlap with the angular profile calculated for a single hole: while the angular dependence for $I_s(\theta)$ has an approximate $\cos^2(\theta)$ profile (dashed curve in Fig. 3.3), our data follow closely the optical power curve $P_s(\theta) \simeq \cos(\theta)$, also plotted in figure as dotted curve. At large angles we note that the expected underestimation of the power is barely noticeable. The good agreement between our measurements and the theoretical curves for the single-hole transmission indicates that we can reconstruct the scattering characteristics of a nano-hole by looking at the collective emission of a series of arrays.

The comparison with theory is not as good for measurements for p-polarization, as Fig. 3.2 shows. In this case the experimental data lie well below the expected curve for the power $P_p(\theta)$, while almost coinciding with the intensity curve $I_p(\theta)$ predicted by Eq. (3.2). The mild shoulders visible in the experimental data around $\theta = 60^\circ$ might still be a remnant of the huge

shoulders predicted for $P_p(\theta)$, which lie outside the figure and occur around $\theta \simeq 75^\circ$ at a value $P(\theta) \simeq 1.86$, but this is highly speculative. The observed discrepancy is not limited to this array: a similar angular profile for transmission in p-polarization was found for a previous sample with the same design but produced independently.

It must be stressed that the CMM expressions are in excellent agreement with full FDTD numerical calculations, but that the theoretical predictions for $p-$polarization also overestimate the radiation at large angles in the case of a *single* hole [20] with a diameter almost twice the one considered in this work. As the radiation in $p-$polarization is more sensitive to the characteristics of SPs, and thus to the properties of the surface, it would be interesting to estimate how the radiation depends on the modification of these properties. One

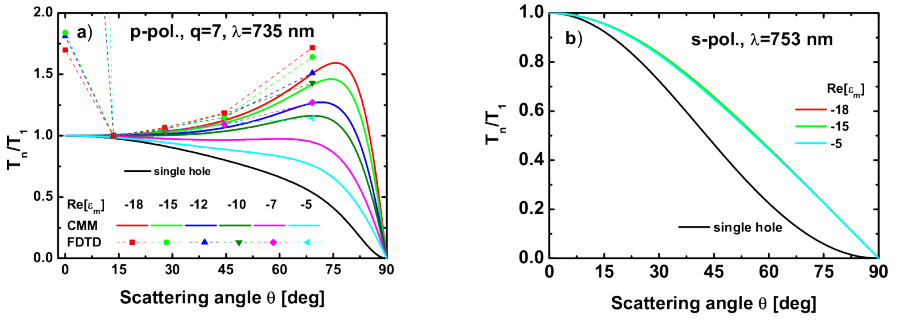

Figure 3.4: Distribution of the transmitted power as a function of angle for different values of Re(ϵ_m), calculated with both CMM model and FDTD; for the latter we show T_n/T_1, transmission per diffraction order normalized by the first diffraction order. Panel (a) is for p-polarization, while panel (b) renders the results for s-polarization.

possibility to explain the discrepancy is a Cr layer thicker than planned. However, our FDTD calculations show that the normalized transmittance remain virtually unchanged even when the thickness of the Cr layer is varied between the values of 5 nm and 25 nm (as a representative example, the intensity of the third order of the q=6 array is reduced by only 2%). Another possibility is that the presence of grains and/or crystal lattice defects in the metal reduces the absolute value of its dielectric constant. Eqs. (3.2)–(3.3) show that a reduction of $|\epsilon_{metal}|$ strongly reduces the p-polarized emission for larger angle with much smaller effects for the s-polarization. We have performed calculations of the radiation pattern as a function of the dielectric constant in the metal (see Fig. 3.4). These simulations show that, in order to reproduce

the experimental pattern, a value $Re(\epsilon_{metal}) \approx -5$ should be used instead of the expected value $Re(\epsilon_{metal}) = -18$. We find that this large modification of the parameters is unrealistic. Similarly, we have performed additional FDTD simulations in which we varied the geometrical parameters of the hole arrays. Some simulations yield a better agreement with the experimental data, but no realistic geometry gave a good fit of the observed anomalous angular profile. Hence, the radiation pattern for p-polarized light is not completely understood.

3.6 Conclusions

In this chapter we have presented the first measurements of the angle-resolved transmission of a set of hole array gratings. We extract the multiple diffraction orders and show how to separate the angular emission profiles of the holes under the excitation of either surface plasmons or normally incident light by applying a known model for extraordinary optical transmission, that we extend describing how to introduce the angular dependence of its coefficients. From the data for hole arrays of different lattice constant, we reconstruct the angular emission properties of a single hole. We compare the experimental results with numerical simulations and an analytical theory for the emission of individual nano-holes in a metal film. While our data for s-polarized excitation are in agreement with the emission profile expected for a single hole, for p-polarized excitation our experiment shows a different profile than theory predicts. We find as possible reason a change of the optical properties of the metal surface inside the hole. Nevertheless the values found for the dielectric constant are not fully satisfactory and an explanation for the observed angular emission requires further study.

We conclude with an outlook and a comment on the use of the EOT model in Eq. (3.1) for the separation of the angular emission properties of the holes subjected to both direct excitation and lateral SP polarization. The separation of the two emission mechanisms was not achievable in our experiment as the complete emission angle on the SP propagation side was not accessible due to total internal reflection at the glass substrate. A future extension of the experiment, with application of the method that we introduced, should thus be performed on SPs propagating at the air side in absence of chromium, or should allow for observation over a larger angular range on the glass side with the use, for instance, of solid immersion lenses. Furthermore, the excitation

of the array at $\theta_{in} \neq 0$ will prevent symmetry from removing interesting contributions to emission via destructive interference of fields from counter propagating SPs.

Acknowledgments

The CMM and FDTD calculations shown in Fig. 3.4 were performed by F. de León-Pérez. FM and MvE are grateful to prof. Eric Eliel and prof. Gert 't Hooft for fruitful discussion and to the AMOLF Institute (Amsterdam) and Dimitry Lamers for support provided in the sample fabrication.

Bibliography

[1] W. L. Barnes, A. Dereux, and T. W. Ebbesen, *Surface Plasmon Subwavelength Optics*, Nature **424**, 824 (2003).

[2] A. A. Yanik *et al.*, *An Optofluidic Nanoplasmonic Biosensor for Direct Detection of Live Viruses from Biological Media*, Nano Letters **10**, 4962 (2010).

[3] H. A. Atwater and A. Polman, *Plasmonics for Improved Photovoltaic Devices*, Nature Materials **9**, 205 (2010).

[4] P. Zijlstra and M. Orrit, *Single Metal Nanoparticles: Optical Detection, Spectroscopy and Applications*, Reports on Progress in Physics **74**, 106401 (2011).

[5] F. J. Garcia-Vidal, L. Martin-Moreno, T. W. Ebbesen, and L. Kuipers, *Light Passing through Subwavelength Apertures*, Reviews of Modern Physics **82**, 729 (2010).

[6] T. W. Ebbesen *et al.*, *Extraordinary Optical Transmission through Sub-Wavelength Hole Arrays*, Nature **391**, 667 (1998).

[7] D. E. Grupp *et al.*, *Crucial Role of Metal Surface in Enhanced Transmission through Subwavelength Apertures*, Applied Physics Letters **77**, 1569 (2000).

[8] A. Degiron, H. J. Lezec, W. L. Barnes, and T. W. Ebbesen, *Effects of Hole Depth on Enhanced Light Transmission through Subwavelength Hole Arrays*, Applied Physics Letters **81**, 4327 (2002).

[9] K. L. van der Molen, F. B. Segerink, N. F. van Hulst, and L. Kuipers, *Influence of Hole Size on the Extraordinary Transmission through Subwavelength Hole Arrays*, Applied Physics Letters **85**, 4316 (2004).

[10] K. J. K. Koerkamp *et al.*, *Strong Influence of Hole Shape on Extraordinary Transmission through Periodic Arrays of Subwavelength Holes*, Physical Review Letters **92**, 183901 (2004).

[11] C. Billaudeau *et al.*, *Angle-Resolved Transmission Measurements through Anisotropic Two-Dimensional Plasmonic Crystals*, Optics Letters **33**, 165 (2008).

[12] M. J. A. de Dood, E. F. C. Driessen, D. Stolwijk, and M. P. van Exter, *Observation of Coupling between Surface Plasmons in Index-Matched Hole Arrays*, Physical Review B **77**, 115437 (2008).

[13] L. Martín-Moreno *et al.*, *Theory of Extraordinary Optical Transmission through Subwavelength Hole Arrays*, Physical Review Letters **86**, 1114 (2001).

[14] H. T. Liu and P. Lalanne, *Microscopic Theory of the Extraordinary Optical Transmission*, Nature **452**, 728 (2008).

[15] G. Gay *et al.*, *The Optical Response of Nanostructured Surfaces and the Composite Diffracted Evanescent Wave Model*, Nature Physics **2**, 262 (2006).

[16] N. Rotenberg *et al.*, *Plasmon Scattering from Single Subwavelength Holes*, Physical Review Letters **108**, 127402 (2012).

[17] H. Liu and P. Lalanne, *Comprehensive Microscopic Model of the Extraordinary Optical Transmission*, Journal of the Optical Society of America A **27**, 2542 (2010).

[18] F. van Beijnum *et al.*, *Quasi-Cylindrical Wave Contribution in Experiments on Extraordinary Optical Transmission*, Nature **492**, 411 (2012).

[19] H. A. Bethe, *Theory of Diffraction by Small Holes*, Physical Review Online Archive (Prola) **66**, 163 (1944).

[20] J. M. Yi *et al.*, *Diffraction Regimes of Single Holes*, Physical Review Letters **109**, 023901+ (2012).

[21] F. de León-Pérez, G. Brucoli, F. J. García-Vidal, and L. Martín-Moreno, *Theory on the Scattering of Light and Surface Plasmon Polaritons by Arrays of Holes and Dimples in a Metal Film*, New Journal of Physics **10**, 105017 (2008).

[22] F. Przybilla *et al.*, *Efficiency and Finite Size Effects in Enhanced Transmission through Subwavelength Apertures*, Optics Express **16**, 9571 (2008).

[23] P. B. Johnson and R. W. Christy, *Optical Constants of the Noble Metals*, Physical Review B **6**, 4370 (1972).